July 2004

Structural Basis and Specificity of Acyl-Homoserine Lactone Signal Production in Bacterial Quorum Sensing

William T. Watson
The University of Colorado Health Sciences Center, Denver CO

Timothy D. Minogue
The University of Connecticut, Storrs CT

Susanne B. von Bodman
University of Connecticut, Storrs CT, susanne.vonbodman@uconn.edu

Dale L. Val
University of Illinois at Urbana-Champaign

Mair E. A. Churchill
The University of Colorado Health Sciences Center, Denver CO

Structural Basis and Specificity of Acyl-Homoserine Lactone Signal Production in Bacterial Quorum Sensing

William T. Watson,[1] Timothy D. Minogue,[2]
Dale L. Val,[3] Susanne Beck von Bodman,[2]
and Mair E.A. Churchill[1]
[1]Department of Pharmacology
The University of Colorado Health Sciences Center
4200 E. Ninth Avenue
Denver, Colorado 80262
[2]Departments of Plant Science and
    Molecular and Cell Biology
University of Connecticut
302 B Agricultural Biotechnology Laboratory
Storrs, Connecticut 06269
[3]Departments of Microbiology and Biochemistry
University of Illinois at Urbana-Champaign
601 S. Goodwin Avenue
Urbana, Illinois 61801

Summary

Synthesis and detection of acyl-homoserine lactones (AHLs) enables many gram-negative bacteria to engage in quorum sensing, an intercellular signaling mechanism that activates differentiation to virulent and biofilm lifestyles. The AHL synthases catalyze acylation of S-adenosyl-L-methionine by acyl-acyl carrier protein and lactonization of the methionine moiety to give AHLs. The crystal structure of the AHL synthase, EsaI, determined at 1.8 Å resolution, reveals a remarkable structural similarity to the N-acetyltransferases and defines a common phosphopantetheine binding fold as the catalytic core. Critical residues responsible for catalysis and acyl chain specificity have been identified from a modeled substrate complex and verified through functional analysis in vivo. A mechanism for the N-acylation of S-adenosyl-L-methionine by 3-oxohexanoyl-acyl carrier protein is proposed.

Introduction

Bacterial quorum sensing systems permit bacteria to sense their cell density and to initiate an altered pattern of gene expression after a sufficient quorum of cells has accumulated (Albus et al., 1977; Fuqua et al., 1994; Sitnikov et al., 1995). Quorum sensing regulates the formation of bacterial biofilms that are associated with a wide variety of chronic infections caused by gram-negative opportunistic bacteria (reviewed in Davies et al., 1998; Whitehead et al., 2001). For example, the biofilm of *Pseudomonas aeruginosa* is made of sessile bacterial colonies encased in polysaccharide matrices that are resistant to antimicrobials and host immune cells. The biofilms severely complicate the treatment of persistently infected cystic fibrosis patients and immune-compromised individuals. Quorum sensing has also been shown to regulate gram-negative bacterial pathogenesis in plants. *Pantoea stewartii*, for example, is a

phytopathogenic bacterium that uses quorum sensing to control the cell density-linked synthesis of an exopolysaccharide (EPS), a virulence factor in the cause of Stewart's wilt disease in maize (Beck von Bodman and Farrand, 1995; Coplin et al., 1992).

Quorum sensing in more than 30 gram-negative bacteria is mediated by lipid signaling molecules that are chemical derivatives of acyl-homoserine lactones (AHLs) (Fuqua and Greenberg, 1998; Swift et al., 1999) (Figure 1A). AHLs are synthesized by AHL synthases, enzymes also known as I proteins, and are sensed by the response regulator family of transcription factors known as R proteins. Intracellular accumulation of a sufficient concentration of the cell-permeable AHL generally leads to activated transcription from different promoters within the bacterial genome by induction of a transcriptionally active response regulator such as LuxR of *Vibrio fischeri* or LasR of *P. aeruginosa* (Pearson et al., 1999; Welch et al., 2000; Zhu and Winans, 2001). However, in several species the response regulator acts as a negative transcriptional regulator (Kanamaru et al., 2000; Lewenza and Sokol, 2001), including EsaR of *P. stewartii* (Beck von Bodman et al., 1998).

Natural and synthetic mechanisms that inhibit or misregulate quorum sensing have detrimental effects on bacterial pathogenicity. *P. aeruginosa* null mutants that lack the AHL synthases, LasI and RhlI, or the response regulator LasR show a decrease in biofilm formation and attenuated pathogenicity in several in vivo infection model systems (Rumbaugh et al., 1999; Tang et al., 1996). In *P. stewartii*, null mutants of the AHL synthase, EsaI, are unable to produce detectable levels of EPS and are less virulent. In contrast, mutants lacking the EsaR response regulator have a hypermucoid phenotype but are also avirulent as a result of constitutive, cell density-independent, EPS synthesis (Beck von Bodman et al., 1998). AHL-specific quorum sensing is inhibited by recently discovered halogenated furanones, produced by the marine alga *Delisea pulchra*, which prevent microbial and metazoan colonization (Hentzer et al., 2002). Production of enzymes that destroy the AHL, such as the N-acyl-homoserine lactonase produced by *Bacillus* species (Dong et al., 2001) or the aminoacylase produced by *Variovorax paradoxus* (Leadbetter and Greenberg, 2000), eliminate quorum sensing and protect the respective hosts from bacterial infection. Finally, ectopic expression of AHL synthases in plant hosts blocks infection of phytobacteria that express virulence functions in an AHL quorum sensing-dependent manner (Fray et al., 1999; Mäe et al., 2001). Therefore, strategies that either inhibit quorum sensing or cause the premature expression of target operons can provide broad-spectrum control of particular bacterial diseases in humans, animals, and plants. To develop synthetic inhibitors of quorum sensing, a better understanding of AHL synthesis is required.

AHLs are produced by the AHL synthase from the substrates S-adenosyl-L-methionine (SAM) and acylated acyl carrier protein (acyl-ACP) in a proposed "biter" sequentially ordered reaction (Parsek et al., 1999;

[1]Correspondence: mair.churchill@uchsc.edu

A

3-oxo-C6-AHL
(EsaI, LuxI)

C4-AHL
(RhlI)

3-oxo-C12-AHL
(LasI)

B

ACP

acyl-acyl carrier protein

+ Adenine

H₃C–S

OH OH

⁺H₃N

S-adenosyl-L-methionine

AHL
synthase

→

acylation

ACP

Adenine

H₃C–S

OH OH

⁺H₃N

lactonization

→

ACP

HS

holo-acyl carrier protein

+ Adenine

H₃C–S

O

OH OH

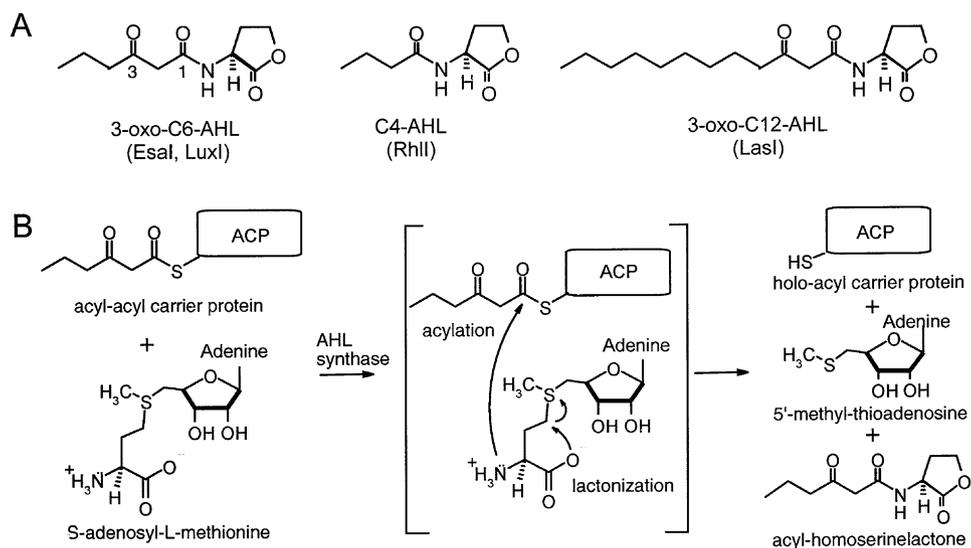5'-methyl-thioadenosine

+

acyl-homoserinelactone

Figure 1. AHL Synthesis

(A) The structures of three AHLs show variation in acyl chain length and degree of oxidation at the acyl chain C3 position.
(B) The schematic diagram illustrates the general features of the AHL synthesis reaction. Two substrates, acyl-ACP and SAM, bind to the enzyme. After the acylation and lactonization reactions, the product AHL and byproducts holo-ACP and 5'-methylthioadenosine are released.

Val and Cronan, 1998) (Figure 1B). In this reaction, the acyl chain is presented to the AHL synthase as a thioester of the ACP phosphopantetheine prosthetic group, which results in nucleophilic attack on the 1-carbonyl carbon by the amine of SAM in the acylation reaction. Lactonization occurs by nucleophilic attack on the γ carbon of SAM by its own carboxylate oxygen to produce the homoserine lactone product. The *N*-acylation reaction, involving an enzyme-acyl-SAM intermediate, is thought to occur first because butyryl-SAM acts as both a substrate and as an inhibitor for the *P. aeruginosa* AHL synthase, RhlI, to produce C4-AHL (Parsek et al., 1999). A unique aspect of the AHL synthesis mechanism is that the substrates adopt roles that differ quite dramatically from their normal cellular functions. SAM usually acts as a methyl donor, whereas acyl-ACPs are components of the fatty acid biosynthetic pathway and had not been implicated in cell-cell communication until their discovery as acyl chain donors in AHL synthesis (Moré et al., 1996). Furthermore, a key step in AHL synthesis is the internal lactonization of SAM, which demands an unusual cyclic conformation that favors this reaction.

AHL synthases from different bacterial species produce AHLs that vary in acyl chain length (from C4 to C14) oxidation at the C3 position and saturation (Fuqua and Eberhard, 1999; Kuo et al., 1994) (Figure 1A). This variability is a function of the enzyme acyl chain specificity and may also be influenced by the available cellular pool of acyl-ACPs (Fray et al., 1999; Fuqua and Eberhard, 1999). More than 40 AHL synthases, similar to the archetype LuxI (Fuqua et al., 1994), have been characterized, and they share four blocks of conserved sequence (Figure 2). Within these blocks, there is on average 37% identity with eight residues that are absolutely conserved. When mutated, the most conserved residues impact catalysis of the LuxI (*Vibrio fischeri*) and RhlI AHL synthases (Hanzelka et al., 1997; Parsek et al., 1997).

Here we present the structure of the AHL synthase, EsaI, determined by X-ray crystallography. The structure, at a resolution of 1.8 Å, provides the basis for the interpretation of past mutagenesis and biochemical results and an understanding of the *N*-acylation step in AHL synthesis. A model of the enzyme-phosphopantetheine complex shows novel interactions important for specificity of AHL synthesis through substrate recognition. The activity and specificity of structure-based mutants, determined from complementary in vivo biological reporter assays, verify the proposed roles of several residues involved in catalysis or enzyme-substrate specificity. Furthermore, we demonstrate the ability to alter the product distribution of the AHL synthase by making a single key mutation. This structure reveals the roles of many conserved residues and provides a mechanistic basis for the first step in AHL synthesis.

Results and Discussion

EsaI Structure

EsaI produces a 3-oxo-hexanoyl-homoserine lactone, which contributes to the quorum-sensing regulation of pathogenicity in *Pantoea stewartii* subsp. *stewartii* (Beck von Bodman and Farrand, 1995). EsaI is representative of the AHL synthase family of proteins, having 28% identity (42% homology) and 23% identity (43% homology) with the *P. aeruginosa* AHL synthases LasI and RhlI, respectively, and preferentially produces an AHL of intermediate length (Figure 1A). The structure of EsaI was determined using X-ray crystallography and is refined at a resolution of 1.8 Å, which is sufficient to identify many ordered water molecules in the active site. A perrhenate-soaked crystal was used to obtain experimental phases by multiple wavelength anomalous diffraction methods (Table 1) (Watson et al., 2001). The refined EsaI model is a mixed α-β fold with a prominent cleft and two well-defined cavities (Figure 3A). Nine heli-

```
        1        •         •         •         •         •         •         •         •         •         •
EsaI    MLELFDVSYEELQTTRSEELYKLRKKTFSDRLGWEVICSQGMES---DEFDGPGTRYILGICEGE---LVCSVRFTSLDRPNMITHTFQHCFSDV--TLPAYGTESSRF
LuxI    MTIMIKKSDFLAIPSEEYKGILSLRYQVFKQRLEWDLVVENNLES---DEYDNSNAEYIYACDDTEN---VSGCWRLLPTTGDYMLKSVFPELLGQQSAPKDPNIVELSRF
LasI     MIVQIGRREEFDKKLLGEHMLKLRAQVFKERKGWDVSVIDEMEI---DGDALSPYYMLIQEDTPEAQVFGCWRILDTTGPYMLKNTFPELLHGKEAPCSPHIWELSRF
RhlI    MIELLSESLEGLSAAMIAELGRYRHQVFIEKLGWDVVTSSRVRDQEFDQFDHPQTRYIVAMSRQG---ICGCARLLPTTDAYLLKDVFAYLCSETP-PSDPSVWELSRY
        = β1       α1         α2                       β2        β3         α3  α4                      β4
tGCN5   LLLDFDILTNDGTHRNMKLLIDLKNIFSRQLPKMPKEYIVKLVF--------DRHHESMVILKNKQK--VIGGICFRQ--------------------YKPQRFAEVAFL
AANAT   NEFRCL----TPEDAAGVFELEREAFISVSGNCPLNLDEVQHFTLCPEL------SLGWFVEGR---LVAFIIGSLWDEER------LTQESLALHRPRGHSAHLHAL
AAC-6'  MIISEFDRN--------------------NPVLKDQL**********ERIAVAAVDQDE---LVGFIGAIP--------------------QYGITGWELHPL
                                              pp                                                            aaap

        102      •         •         •         •         •         •         •         •         •         •
EsaI    FVDKARARALLGEHYPISQVLFLAMVNWAQNNAYGNIYTIVSRAMLKILTRSGWQIKVIK--EAFLTEKERIYLLTLPAGQDDKQQLGGDVVSRTGCPPVAVTTWPLTLPV
LuxI    AVGKNSSKINNSASEITMK--LFEAIYKHAVSQGITEYVTVTSTAIERFLKRIKVPCHRIGDKEIHVLGDTKSVVLSMPINEQFKKAVLN
LasI    AINSGQKGSLGFSDCTLE--AMRALARYSLQNDIQTLVTVTTVGVEKMMIRAGLDVSRFG--PHLKIGIERAVALRIELNAKTQIALYGGVLVEQRLAVS
RhlI    AASAADD------PQLAMK-IFWSSLQCAWYLGASSVVAVTTTAMERYFVRNGVILQRLG--PPQKVKGETLVAISFPAYQERGLEMLLRYHPEWLQGVPLSMAV
        β4      α5          α6          β5      α7         β6          β7           α8          α9   β8
tGCN5   AVTANE------QVRGYGTRLMNKFKDHMQKQNIEYLLTYADNFAIGYFKK--QGFTKEH**********GTLMECYIH
AANAT   AVHRSF------RQQGKGSVLLWRYLHHVGAQPVRRAVLMCEDALVPFYQR--FGFHPAGP********LTFTEMHCSL
AAC-6'  VVESS------RRKNQIGTRLVNYLEKEVASRGGITIYLGTD*HPYEFYEK--LGYKIVGVLP***GWKPDIWMAKTII
        pp          ppppppp                  aa p  p  pp
```
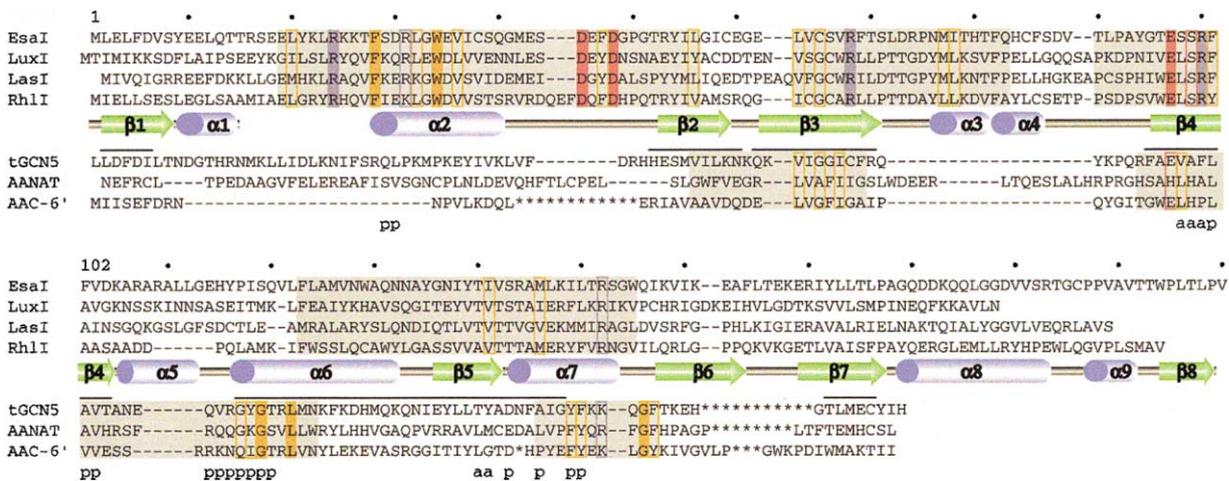
Figure 2. Sequence and Structural Alignment of Selected AHL Synthases and GNATs

The sequence and topology of the AHL synthase family is compared to the GCN5-related N-acetyltransferases. The gray shaded regions are conserved sequence blocks within each family that constitute the enzyme's "sequence signature." Residues are colored red to indicate acidic or hydrophilic, blue for basic, and orange for other. Shaded residues are absolutely conserved, and the boxed residues are homologous within each family. Residues that comprise the core "phosphopantetheine binding fold" were identified by LSQMAN using a 2.0 Å cutoff and are indicated by black bars above the segments. The *Tetrahymena* GCN5 residues that contact the pantetheine or acetyl portion of the acetyl-CoA are indicated by "p" or "a," respectively.

ces surround a highly twisted eight-stranded β sheet, forming a V-shaped active-site groove (Figures 2 and 3A). Helices 1 and 2 are relatively disordered in the crystal, and the loop between them, residues 16–28, has not been built. This region is highly mobile as indicated by significantly higher than average B factors. Interest-

ingly, this site features three of the absolutely conserved residues, Arg24, Phe28, and Trp34, which suggests that a conformational change or stabilization of this conserved region will occur when substrates bind.

To identify the enzyme active site, the relative degree of sequence conservation across the entire AHL syn-

Table 1. Structure Determination and Refinement Statistics

Phasing Statistics	Native	R3-λ1	Re-λ2	Re-λ3	Re-λ4
Wavelength (Å)	1.00	1.14	1.1724	1.1719	1.19
Resolution (Å)	99–1.8	30–2.5	30–2.7	30–2.7	30–2.5
High-resolution shell (Å)	(1.86–1.80)	(2.6–2.5)	(2.8–2.7)	(2.8–2.7)	(2.6–2.5)
Observed reflections	174,794	32,922	28,546	28,071	36,442
Unique reflections	19,521	7283	5764	5772	7313
Completeness (%)	96.5 (92.0)	97.0 (98.1)	97.6 (98.7)	97.7 (98.9)	96.9 (99.5)
Redundancy	9.0	4.5	5.0	4.9	5.0
R_{sym}[a]	3.9 (19.5)	4.2 (17.5)	4.8 (14.8)	5.7 (17.6)	3.3 (17.9)
$<I/\sigma>$	48.5 (5.2)	20.9 (4.7)	11.5 (6.3)	17.7 (3.8)	26.6 (5.2)
Overall Z score[b]		19.0			
Figure of merit after phasing[b]		0.33			
Figure of merit after solvent flattening[c]		0.57			

Refinement Statistics	
Resolution range (Å)	30–1.8 (1.86–1.80)
R value (%)[d]	20.9 (25.1)
Free R value (%)[e]	24.3 (29.6)
Number of reflections used	18,828
Luzatti coordinate error (Å)	0.23

Model	Protein	Solvent
Number of atoms	1550	100
Average B factor (Å²)	35.6	42.9
RMSD bond lengths (Å)	0.0092	
RMSD bond angles (°)	1.35	

[a] $R_{sym} = \Sigma_i |I_i - \langle I \rangle| / \Sigma_i I_i$, where $\langle I \rangle$ is the mean intensity for equivalent reflections, I_i.
[b] Calculated by SOLVE.
[c] Calculated by RESOLVE.
[d] R value = $\Sigma ||F_o| - |F_c|| / \Sigma |F_o|$.
[e] Free R value calculated with an excluded set of 1851 reflections (9.5%).
[f] Space group p4₃; MAD unit cell dimensions (Å): a = b = 66.40, c = 47.33; native unit cell dimensions (Å): a = b = 66.99, c = 47.01.
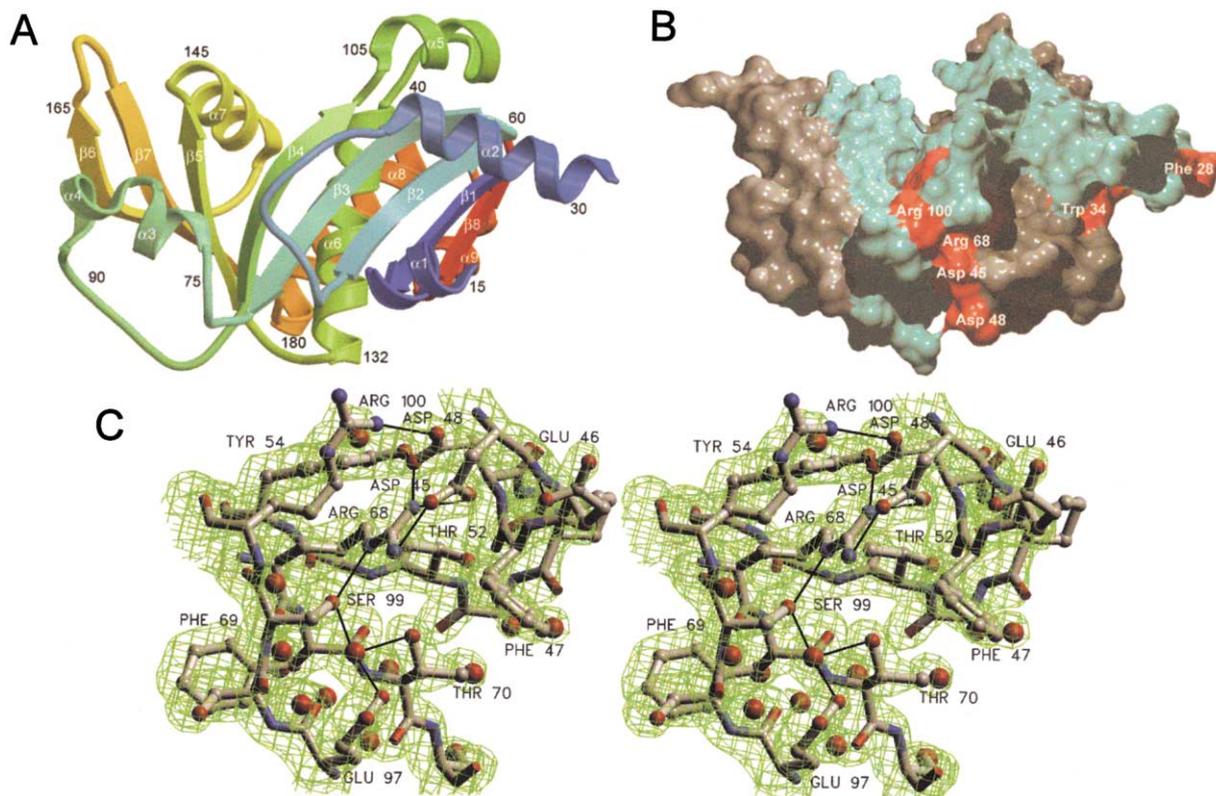
Figure 3. Structure of EsaI

(A) A ribbon diagram, colored from blue to red, indicates the N- to C-terminal positions of residues within the sequence.

(B) AHL synthase absolutely conserved residues shown in red, homologous residues in cyan, and nonhomologous residues in gray are depicted on a surface rendering of EsaI.

(C) Electrostatic cluster of conserved residues. Asp45, Asp48, Arg68, Glu97, and Arg100 form a cluster of electrostatic interactions with each other, Ser99, and a well-ordered water molecule, as indicated by the black lines in stereoview. The 2Fo-Fc electron density map, calculated using CNS, was contoured at 1.5 σ. These figures were prepared using MOLSCRIPT (Kraulis, 1991), Raster3D, VMD, SETOR (Evans, 1993), and Photoshop (Adobe).

thase family was mapped on the surface of the EsaI structure (Figure 3B). All of the homologous residues lie on the same face of the enzyme and are localized either to an apparent active site cleft or the disordered N terminus. The conserved residues at the N terminus are hydrophobic or charged, and reside in the block of the AHL synthase family that has the least sequence variability, supporting earlier proposals that SAM and ACP interact with this region (Hanzelka et al., 1997; Parsek et al., 1997). The remainder of the conserved residues, Asp45, Asp48, Arg68, Glu97, and Arg100, cluster into a network of ion pairs that stabilize the interaction of the N-terminal domain at the coil between α2 and β2 (Figure 3C). Ser99 is a key residue at the center of this cluster and interacts directly with Arg68 and a bridging water molecule bound to Glu97. Ser99 is conserved as either serine or threonine in all known LuxI-like AHL synthases, but only Asp45 and Glu97 had previously been shown to be essential for AHL synthesis in LuxI and RhlI (Hanzelka et al., 1997; Parsek et al., 1997). The longstanding hypothesis that the reaction mechanism of AHL synthesis by LuxI-like AHL synthases involves a covalent thio-acyl-enzyme intermediate through an active-site cysteine is disproved by the EsaI structure. There are no cysteine residues accessible to the substrates in the AHL syn-

thase active site, unlike enzymes involved in fatty acid biosynthesis.

Phosphopantetheine Binding Fold
A close structural relationship with a family of enzymes unrelated by sequence provides insight into the mechanism of AHL synthesis. The EsaI structure has the same fold as the *N*-acetyltransferases with greatest similarity to *Tetrahymena* GCN5 (PDB entry 1QSR) for which a DALI score of 11 is observed (Holm and Sander, 1996). The core fold, defined as the residues that superimpose to within 2 Å, has an rms deviation of 0.9 Å over the Cα positions of 71 residues. There is virtually no sequence similarity between EsaI and the GCN5-related *N*-acetyltransferase (GNAT) enzyme family with the exception of Val103, which contacts the phosphopantetheine portion of acetyl-CoA in GCN5. The structural alignment in Figure 2 shows the common features of the phosphopantetheine fold. Particularly, β strands β2, β3, β4, and β5 and the cleft between β4 and β5 coincide with residues in the GNATs that are involved in acetyl-CoA binding and catalysis of the lysine acetylation reaction. The proposed enzymatic reaction of AHL synthesis is similar to *N*-acetylation, where the amine moiety of the SAM is the nucleophile and the carbonyl carbon of the acyl-

ACP is the electrophile. In addition to similarities in phosphopantetheine binding cleft, the AHL synthases and GNAT enzymes have similarly mobile N-terminal domains. Implications of this fold similarity are that mechanistic features such as substrate binding, catalysis, and regulation of enzyme activity will also be similar.

The observation of a common core fold in EsaI and the GNATs redefines the function of this fold on a structural and evolutionary basis as a phosphopantetheine binding domain. However, the phosphopantetheine binding fold of the GNATs and AHL synthases differs significantly from other enzymes that bind phosphopantetheine, such as phosphopantetheine adenylyltransferase (Izard and Geerlof, 1999). Although the common N-acylation function of the domain was recognized, distinguishing this fold from the phosphopantetheine adenylyltransferases, there was no detectable sequence similarity or structural relationship prior to the structure determination of EsaI reported here. Interestingly, the lack of phosphopantetheine-related sequence conservation among all of these enzymes is due to the finding that all of the intermolecular hydrogen bonds involve protein main chain atoms.

Substrate Modeling
The high degree of structural similarity between the GNATs and AHL synthases permitted the modeling of the 3-oxo-hexanoyl phosphopantetheine of acyl-ACP into the active site of EsaI (Figures 4A and 4B). In both acyl-ACP and acetyl-CoA, the terminal thiol of phosphopantetheine forms a thioester bond to either a variable length acyl chain or an acetyl group. Holo- and acyl-ACP carry phosphopantetheine via a phosphodiester bond to the hydroxyl oxygen atom of Ser36. In acetyl-CoA, however, phosphopantetheine forms a pyrophosphate linkage to the 5′ phosphate of adenosine 3′5′-diphosphate. The common phosphopantetheine portion of acetyl-CoA in the GCN5-acetyl-CoA complex (Rojas et al., 1999) and the S-acetyltryptamine-serotonin N-acetyltransferase (AANAT)-bisubstrate complex (Hickman et al., 1999a) occupies the central catalytic cleft that is highly conserved structurally with EsaI (Figures 2 and 4B). Charge stabilization of the substrate in the modeled complex will occur from positively charged residues that line this surface of EsaI and from Lys105, which folds over the top of the phosphate group of the modeled substrate. Hydrophobic interactions stabilize the acyl-phosphopantetheine carbon chain near Leu118, Ser119, and Met146 of EsaI. There is a "β bulge" distortion in β strand 4 at residues 99 and 100, due in part to hydrophobic packing interactions of Val103, which positions Val103 to form a critical hydrogen bond between the backbone amide and the carbonyl at position 5 of phosphopantetheine. The Phe101 side chain is similarly packed toward the hydrophobic core, positioning its carbonyl as a hydrogen bond acceptor for the N3 of phosphopantetheine. The β bulge also places the backbone amides of residues 100 and 101 within hydrogen bonding distance of the acyl C1 carbonyl oxygen that will form an oxyanion during the acylation reaction.

AHLs vary greatly in acyl chain length from the C4-AHL, produced by *P. aeruginosa* RhlI, to the 7-cis-C14-AHL, produced by *Rhodobacter sphaeroides* CerI

(Puskas et al., 1997). To determine which features of the structure are important for acyl chain length recognition, we analyzed the acyl chain position and contacts in the EsaI-phosphopantetheine model. The 3-oxo-hexanoyl portion of the modeled substrate fits neatly into a hydrophobic cavity in EsaI and interacts with conserved residues that position it in the proper orientation for catalysis. Ser98, Met126, Thr140, Val142, Met146, and Leu176 line this pocket, which is surrounded by seven well-ordered water molecules (average B factor of 24.1) (Figure 4B). Numerous other residues within the protein core but not necessarily in direct contact with the hexanoyl chain direct the size and shape of the cavity through hydrophobic packing, including Phe123, Ser143, Met146, Ile149, Leu150, Ser153, Trp155, Ile157, and Ala178. The homologous AHL synthase of *P. aeruginosa*, LasI, produces a significantly longer AHL, 3-oxo-dodecanoyl-homoserine lactone, and when the residues in the cavity of EsaI were modeled as the corresponding residues of LasI in their most favorable energetic conformations, the binding cavity expanded in length and width (data not shown). This observation suggests that different length acyl chains may be accommodated by coordinated sequence differences in and near the binding pocket.

AHLs produced by different bacterial species also vary in the degree of oxidation at the AHL C3 position. The preference for unsubstituted-, 3-oxo-, or 3-hydroxy-acyl-ACPs is thought to be due to the intrinsic selectivity of the AHL synthase for a particular subset of a pool of available acyl-ACP substrates. For example, the AHL synthase, LasI, produces predominantly 3-oxo-C12-AHL, whereas RhlI produces an unsubstituted C4-AHL from the same cellular pool of acyl-ACPs. We examined the structural basis for the preference of EsaI for 3-oxo-substituted acyl-ACP substrates and found that there is a predicted hydrogen bond between the C3 carbonyl in 3-oxo-hexanoyl-ACP and the Thr140 hydroxyl of EsaI. This interaction may provide added affinity for 3-oxo-acyl-ACPs over other forms of acyl-ACP and suggests the explanation for the preference of EsaI for a 3-oxo-substituted acyl chain substrate.

Enzyme Activity and Substrate Specificity
We confirmed the contributions of individual residues to enzyme activity predicted by the EsaI-acyl-phosphopantetheine model using biological assays. Site-specific mutations in the *esaI* gene altering these and other important residues were evaluated by a TLC bioassay using the Agrobacterium tumefaciens and Chromobacterium violaceum bioreporter systems (Cha et al., 1998; McClean et al., 1997). The wild-type enzyme produces primarily the 3-oxo-C6 AHL and lesser amounts of the 3-oxo-C8 and 3-oxo-12 AHLs (Figure 5A). The Chromobacterium bioassay, which is more specific for detecting the alkanoyl-AHL species, indicates that native EsaI produce small amounts of C6-AHL and C8-AHL (Figure 5B). Residues Asp45 and Glu97 were expected to affect enzymatic activity based on their conservation and previous studies (Hanzelka et al., 1997; Parsek et al., 1997). As predicted, the substitution D45N greatly impairs the enzymatic activity of EsaI with no AHLs detected in either bioassay, and the E97Q substitution dramatically
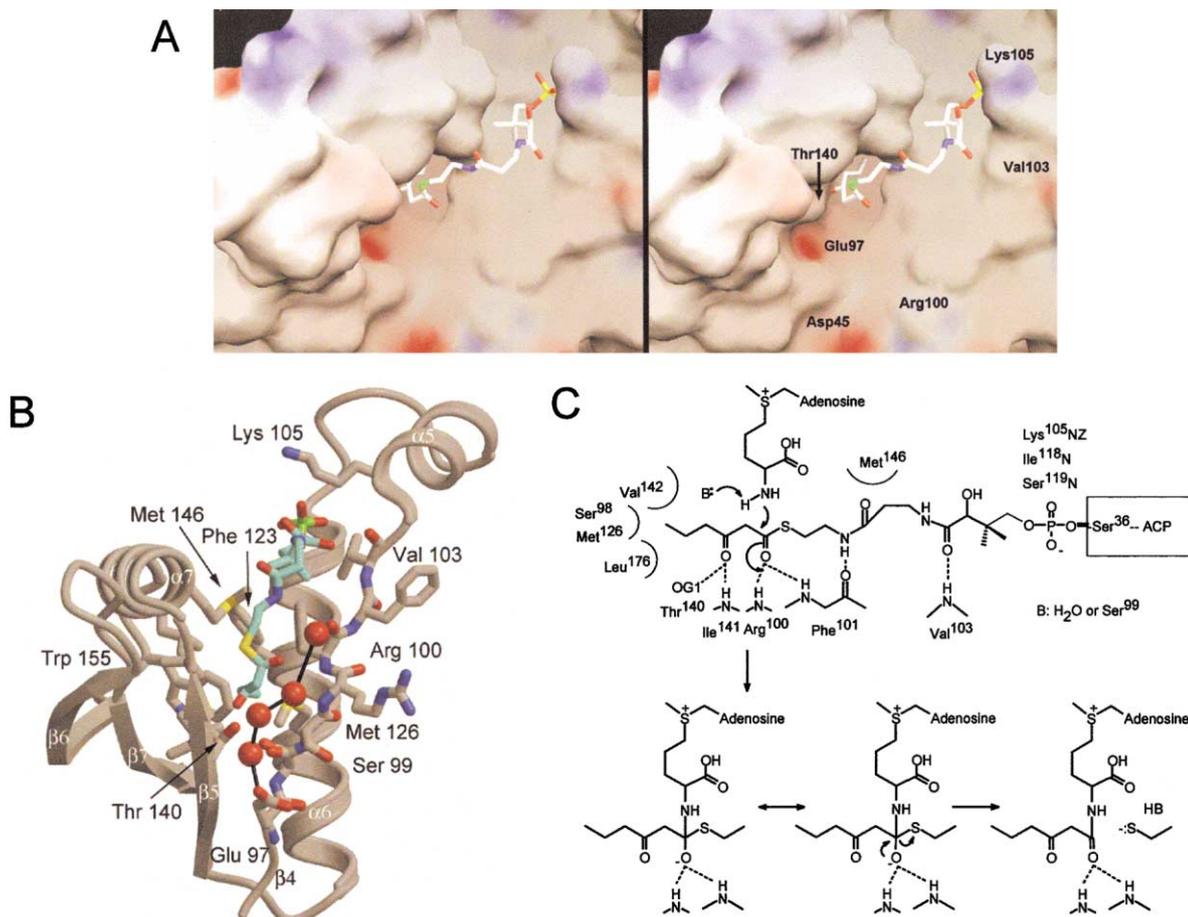
Figure 4. Proposed Mechanism of Acyl Transfer

(A) The stereodiagram of acyl-phosphopantetheine modeled into the Esal active-site cavity viewed as in Figure 2A. The electrostatic surface, generated using GRASP (Nicholls et al., 1993) and Photoshop (Adobe), is colored red, white, and blue to indicate negatively charged, neutral, or positively charged regions of the surface, respectively. The individual atoms in the modeled phosphopantetheine are colored according to atom type.

(B) The acylation cleft of Esal and relevant residues are shown in gray, the modeled phosphopanteteine is shown in cyan, and the well-ordered water molecules observed in the native structure that lie along β4 are shown as red spheres.

(C) The proposed N-acylation reaction is catalyzed via nucleophilic attack on the 1-carbonyl of acyl-ACP by the free amine electrons of SAM after proton abstraction by a water molecule stabilized by Glu97 or Ser99.

impacts enzymatic function yielding only minor amounts of 3-oxo-C6 AHL (Figure 5A). The Esal-phosphopantetheine model also predicts that Ser99 plays an important role in the acylation reaction. This is confirmed by the residue substitution S99A that results in a reduction of activity that is equivalent to the most deleterious Esal mutations. That these mutants are catalytically deficient suggests that the electrostatic cluster of conserved charged residues is important either for catalysis or structural integrity of the active site.

Mutations designed by analysis of the model confirmed the location of the acyl chain binding region of the active site and the mechanism of specificity for C3-substituted acyl-ACP. Among the mutations designed to alter the chain-length specificity of Esal, F123M, which would increase the size of the acyl chain cavity, had no appreciable effect on either enzyme activity or substrate specificity, whereas the T140V substitution, which would decrease access to the cavity, produced a catalytically compromised enzyme (Figure 5A). In contrast,

the T140A substitution, which was predicted to influence the preference for substrates oxidized at the C3 position, produced an active enzyme with altered substrate specificity. T140A exhibited reduced synthesis of the 3-oxo-AHLs (Figure 5A) and increased synthesis of alkanoyl-C6 AHL (Figure 5B). Esal, Lasl, and Luxl all have a conserved threonine at this position and preferentially react with 3-oxo-acyl ACPs to produce 3-oxo-AHLs. *Rhizobium leguminosarum* Cinl has a serine at this position and produces N-(3-hydroxy-7-cis-tetradecenoyl)-L-homoserine lactone (Lithgow et al., 2000). Rhll, Cerl, Swrl, and Asal are examples of AHL synthases that preferentially produce AHLs that lack a 3-oxo or 3-hydroxy moiety (Fuqua and Eberhard, 1999), and these invariably have either alanine or glycine at the position equivalent to T140 in Esal. This analysis reveals that the identity of the residue at position 140 accounts in part for the different C3 substitutions in AHLs produced by AHL synthases of different bacterial species. In contrast, acyl chain length selectivity is more complex, requiring a
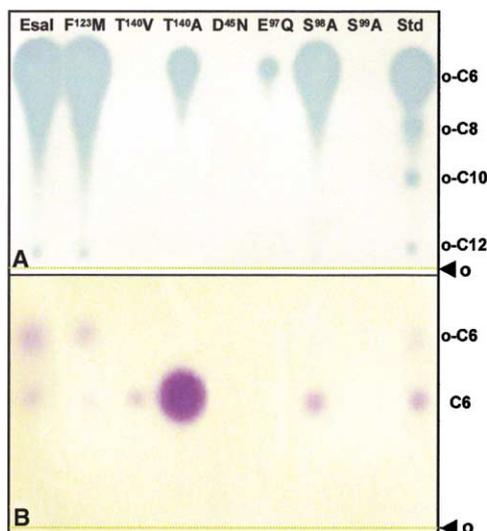
Figure 5. C_{18} Thin-Layer Chromatography (TLC) Bioassays Indicate Residues Important for Activity and Specificity

Ethyl acetate preparations were applied to the origin (o) of the TLC plate.

(A) *A. tumefaciens* bioassay (Cha et al., 1998). Standards (Std) are synthetic preparations of *N*-3-oxo-AHLs indicated by their respective acyl side chains (o-C12, o-C10, o-C8, and o-C6). A 3 μl volume each for the wild-type, and F123M, T140V, and T140A mutants, and 5 μl each for mutants D45N, E97Q, S98A, and S99A was used.

(B) *C. violaceium* bioassay using 6 μl volumes of each ethyl acetate preparation (McClean et al., 1997; Swift et al., 1997). Standards are o-C6 and alkanoyl C6 (gift from Michael A. Savka).

larger number of sequence changes and possibly also structural changes to accommodate acyl-ACPs of different acyl chain lengths.

Proposed Mechanism of Acylation

The structural and mechanistic similarities between the AHL synthases and the GNATs suggest an enzymatic mechanism for the AHL synthases (Figure 4C). The V-shaped clefts formed by the separation of strands β4 and β5 positions the surface side chains to surround the phosphopantetheine in nearly the same way for the modeled EsaI complex as for AANAT and GCN5 (Figure 3A). The mechanism of acylation in the GNATs requires a catalytic base to abstract a proton from the amine nitrogen so that nucleophilic attack can occur on the C1 carbonyl carbon of acetyl-CoA. This is accomplished by a unique active-site structure. In the GNATs, a conserved β bulge, which occurs at Leu121 and His122 in AANAT (Hickman et al., 1999a, 1999b) and at Val123 and Ala124 in tGCN5 (Rojas et al., 1999), positions two adjacent carbonyl oxygen atoms to coordinate a well-ordered water molecule. The β-bulge in EsaI occurs at residues 99 and 100, offset by one residue toward the C terminus compared with the β-bulge in AANAT and GCN5. This structure enables proton abstraction from the protonated amine of the substrate by a catalytic base. In addition, the EsaI β-bulge positions the backbone amides of Arg100 and Phe101 toward the C1 carbonyl oxygen atom of the acyl chain forming a potential carboxyanion hole that would stabilize the negatively charged oxygen atom during catalysis.

The precise identity of the catalytic base in the EsaI structure is not obvious. Evidence from studies with AANAT suggest that the catalytic base may be a water molecule that is aided by a "proton wire" comprised of eight water molecules, the β bulge carbonyl oxygens, and residues His120 and His122 (Hickman et al., 1999a) acting as an electrostatic sink. The catalytic base in GCN5 was determined to be Glu120 (Tanner et al., 1999). In EsaI, Ser99 is in the same position as His122 in AANAT, which was shown to be important in proton abstraction from the protonated amine by stabilizing the putative hydronium ion. Ser99 is essential for catalysis in EsaI (Figure 5). The side chain Ser99 points into the ion pair cluster away from the acyl-carbonyl, but even a very minor conformational change could position the Ser99 hydroxyl to face toward the acyl chain, allowing it to hydrogen bond with the waters present in the active site groove. An alternative catalytic base, EsaI Glu97, adopts the same position as the Glu120 in GCN5 and His120 in AANAT, and a network of well-ordered water molecules, or proton wire, connects the substrate model to this residue (Figure 4B). Glu97 lies at the base of a large electronegative cavity and may be instrumental in imparting a charge gradient across the water molecules, one of which may act as the catalytic base. In this model, Glu97 is unlikely to be the catalytic base itself because it is too far, >8 Å, from the site of nucleophilic attack, the C1 position of acyl-ACP. The site of SAM amine deprotonation is expected to be within a couple of angstoms from the C1 position, which is still too far for direct interaction with Glu97. However, Glu97 may act directly as the catalytic base if there is a conformational change that would bring the amine of SAM in close proximity. Thus, the mechanism of acylation in AHL synthesis is likely to be similar to that observed for *N*-acetylation by two different subfamilies of enzymes of the GNAT family.

The acetylation mechanism of AANAT and GCN5 sheds light on the molecular basis for ordered substrate binding. The apo-EsaI structure exists in an "open conformation" with an exposed deep cavity that can easily accommodate the acyl-phosphopantetheine-chain of acyl-ACP without requiring any major conformational change. However, the unstructured wing of the enzyme and the conserved residues that lie in this region argue for a conformational change upon acyl-ACP and/or SAM binding that would alter the detailed structure of the catalytic core and possibly reorient the active site Ser99. The loop between α1 and α2 contains three absolutely conserved residues and exists in the native protein as a highly flexible region. This region is the most structurally variable and can be found in a variety of conformations among the GNAT structures. For example, in AANAT this region, α1–α2, undergoes substantial conformational changes after acetyl-CoA binds (Hickman et al., 1999b). The homologous loop of AANAT has been shown to act as a regulatory region in the 14-3-3 proteins, which structurally modulate the substrate binding sites, measurably increasing the affinity of AANAT for its substrates in a bi-bi sequentially ordered mechanism (Obsil et al., 2001). EsaI is capable of forming complexes with both holo-ACP and acyl-ACP in vitro as seen in native polyacrylamide gel shift assays in the absence of exogenous SAM (data not shown). Furthermore, the helical

structure of ACP resembles that of 14-3-3, which suggests that this region of the enzyme may be important in ACP recognition and binding. Therefore, it is likely that the AHL synthase binds acyl-ACP first, followed by a conformational rearrangement of the N-terminal domain and SAM binding in a bi-ter sequentially ordered mechanism.

Conclusions

The Esal structure reveals that the core catalytic fold of the AHL synthase family has features essential for phosphopantetheine binding and *N*-acylation that are similar to the GNAT family of N-acetyltransferases. The modeling study and GNAT structural analysis suggests that the reaction mechanism of the first step in AHL-mediated quorum sensing signal generation, the *N*-acylation reaction of SAM, is also likely to include a similar type of amine proton abstraction by a catalytic base. In addition, variable residues in the C-terminal half of the protein and the presence or absence of a Ser/Thr at position 140 constitute the basis for the acyl chain specificity. Other enzymes in gram-negative bacteria that synthesize lipid communication signals, such as the LuxM-type AHL synthases (for example, LuxM, AinS, and VanM [Hanzelka et al., 1997, 1999; Parsek and Greenberg, 2000; Parsek et al., 1997]) also appear to share some sequence homology with Esal, particularly in the conserved block 3 catalytic region. Not surprisingly, a novel quorum-sensing system, mediated by the LuxS and LuxP gene products, which synthesizes and responds to the AI-2 molecule (Chen et al., 2002; Lewis et al., 2001), is distinct chemically and structurally from the AHL-mediated system described here.

Understanding the molecular mechanisms underlying quorum sensing at the atomic level will greatly enhance the ability to design new inhibitory compounds to fight pathogenic bacteria of many different species. Recent studies in vivo have shown that the virulence of *P. aeruginosa* lacking one or more genes responsible for AHL-mediated quorum sensing is attenuated in its ability to colonize and spread within the host (Rumbaugh et al., 1999). Similarly, elimination of the AHL synthase in several plant pathogenic bacteria has led to complete loss of infectivity (Beck von Bodman et al., 1998; Whitehead et al., 2001). Moreover, ectopic expression of AHL synthases in transgenic plant systems has demonstrated that when invading bacteria encounter inducing levels of AHLs their behaviors are sufficiently modulated to shift the delicate balance of host-microbe interactions in favor of disease resistance (Fray et al., 1999; Mäe et al., 2001). A number of plants, including common crop plants, produce endogenous AHL compounds, and it is thought that these AHLs are the basis of varying degrees of disease resistance and susceptibility (Teplitski et al., 2000). Certainly, the halogenated furanones produced by some marine algae have a pronounced effect on suppressing marine biofouling. These examples all underscore the potential to control a wide range of bacterial diseases and biofilm formation in industrial, medical, and ecological settings. Therefore, this AHL synthase structure sets the stage for future structure-based approaches to develop novel inhibitors to fight persistent biofilm-mediated infections (Finch et al., 1998) and bio-

film-based ecological problems specifically due to gram-negative bacteria (Dalton and March, 1998).

Experimental Procedures

Protein Production and Purification

Esal was overexpressed in *E. coli* from a pET 14b-based vector, pET14b-*esal*, as described previously (Watson et al., 2001). The protein was purified from the soluble fraction of the bacterial cell lysate using Ni-NTA (Qiagen) column chromatography with an imidazole gradient. After dialysis into 20 mM HEPES (pH = 7.5), 0.3 M NaCl, and 10 mM DTT, the Esal protein is approximately 95% pure by Coomassie-stained SDS-PAGE and mass spectrometry (data not shown). The purified protein was stored by flash freezing in liquid N_2 and thawed on ice prior to crystallization trials.

Structure Determination and Refinement

Crystals were grown by vapor diffusion in a drop composed of 7 μl Esal (6 mg/mL) and an equal volume of the crystallization well solution (0.1 M MES [pH = 6.1], 14% PEG 4000, 6% isopropanol, 0.03% β-mercaptoethanol, 10 mM EDTA, and 0.5% NaN₃) as described previously (Watson et al., 2001). The structure was solved by MAD with a single ammonium perrhenate-soaked crystal using SOLVE and RESOLVE, as described elsewhere (Studier et al., 1990; Watson et al., 2001). The model was built using O (Jones et al., 1991), and iterative model refinement, energy minimization, simulated annealing, and individual B factor refinement were carried out using CNS (Brünger et al., 1998). Model bias was removed during refinement using overlapping simulated annealing omit maps and composite simulated annealing omit maps. Stereochemistry was analyzed using PROCHECK (Laskowski, 1993), with 92.7% of phi/psi angles lying in the most favored regions of the Ramachandran plot. Water molecules were placed between 2.4–3.4 Å from any hydrogen acceptor or donor atoms in significant peaks in an Fo-Fc map. Analysis programs (CNS and CCP4) were used to evaluate the stereochemistry of the protein model and crystal contacts (Brünger et al., 1998; Laskowski, 1993). The acyl-phosphopantetheine model was refined into the active-site cavity of a rigid model of Esal using CNS (Brünger et al., 1998).

Mutagenesis and Bioreporter Assays

Single residue mutations were created using the Stratagene Quik-Change site-directed mutagenesis kit and the wild-type pET14b-*esal* (Beck von Bodman and Farrand, 1995; Watson et al., 2001) construct as a DNA template (each mutation was confirmed by automated DNA sequencing). The relative activity of the mutant Esal enzymes was analyzed by C_{18} thin-layer chromatography (TLC) bioassay using established methods for the *A. tumefaciens* reporter strain NT1(pZLR4) (Cha et al., 1998) and *C. violaceum* strain CV02blu (McClean et al., 1997; Swift et al., 1997). AHLs were extracted with equal volumes of ethyl acetate from culture supernatants of *E. coli* DH5α cultures expressing either the wild-type Esal or the separate mutants as hexa-histidine-tagged fusion proteins. The samples were concentrated 10-fold before spotting on the TLC plates.

References

Albus, A.M., Pesci, E.C., Runyen-Janecky, L.J., West, S.E., and Iglewski, B.H. (1977). Vfr controls quorum sensing in *Pseudomonas aeruginosa*. J. Bacteriol. *179*, 3928–3935.

Beck von Bodman, S., and Farrand, S.K. (1995). Capsular polysaccharide biosynthesis and pathogenicity in *Erwinia stewartii* require induction by an N-acylhomoserine lactone autoinducer. J Bacteriol. *177*, 5000–5008.

Beck von Bodman, S., Majerczak, D.R., and Coplin, D.L. (1998). A negative regulator mediates quorum-sensing control of exopolysaccharide production in *Pantoea stewartii* subsp. *stewartii*. Proc. Natl. Acad. Sci. USA *95*, 7687–7692.

Brünger, A.T., Adams, P.D., Clore, G.M., DeLano, W.L., Gros, P., Grosse-Kunstleve, R.W., Jiang, J.-S., Kuszewski, J., Nilges, M., Pannu, N.S., et al. (1998). Crystallography & NMR system: a new software suite for macromolecular structure determination. Acta Crystallogr. *D54*, 905–921.

Cha, C., Gao, P., Chen, Y.C., Shaw, P.D., and Farrand, S.K. (1998). Production of acyl-homoserine lactone quorum-sensing signals by gram-negative plant-associated bacteria. Mol. Plant Microbe Interact. *11*, 1119–1129.

Chen, X., Schauder, S., Potie, N., Van Dorsselaer, A., Pelczer, I., Bassler, B.L., and Hughson, F.M. (2002). Structural identification of a bacterial quorum-sensing signal containing boron. Nature *415*, 545–549.

Coplin, D.L., Frederick, R.D., Majerczak, D.R., and Tuttle, L.D. (1992). Characterization of a gene cluster that specifies pathogenicity in *Erwinia stewartii*. Mol. Plant Microbe Interact. *4*, 81–88.

Dalton, H.M., and March, P.E. (1998). Molecular genetics of bacterial attachment and biofouling. Curr. Opin. Biotechnol. *9*, 252–255.

Davies, D.G., Parsek, M.R., Pearson, J.P., Iglewski, B.H., Costerton, J.W., and Greenberg, E.P. (1998). The involvement of cell-to-cell signals in the development of bacterial biofilm. Science *280*, 295–298.

De Kievit, T.R., and Iglewski, B.H. (2000). Bacterial quorum sensing in pathogenic relationships. Infect. Immun. *68*, 4839–4849.

Dong, Y.-H., Wang, L.-H., Xu, J.-L., Zhang, H.-B., Zhang, X.-F., and Zhang, L.-H. (2001). Quenching quorum-sensing-dependent bacterial infection by an N-acyl homoserine lactonase. Nature *411*, 813–817.

Evans, S. (1993). SETOR: hardware lighted three-dimensional solid model representations of macromolecules. J. Mol. Graph. *11*, 134–138.

Finch, R.G., Pritchard, D.I., Bycroft, B.W., Williams, P., and Stewart, G.S.A.B. (1998). Quorum sensing: a novel target for anti-infective therapy. J Antimicrob. Chemother. *42*, 569–571.

Fray, R.G., Throup, J.P., Daykin, M., Wallace, A., Williams, P., Stewart, G.S., and Grierson, D. (1999). Plants genetically modified to produce N-acylhomoserine lactones communicate with bacteria. Nat. Biotechnol. *171*, 1017–1020.

Fuqua, C., and Eberhard, A. (1999). Signal generation in autoinduction systems: synthesis of acylated homoserine lactones by LuxI-type proteins. In Cell-Cell Communication in Bacteria., G. Dunny and S.C. Winans, eds. (Washington: AMS Press), pp. 211–230.

Fuqua, W.C., and Greenberg, E.P. (1998). Self-perception in bacteria: quorum sensing with acylated homoserine lactones. Curr. Opin. Microbiol. *1*, 183–189.

Fuqua, W.C., Winans, S.C., and Greenberg, E.P. (1994). Quorum sensing in bacteria: the LuxR-LuxI family of cell density-responsive transcriptional regulators. J. Bacteriol. *176*, 269–275.

Hanzelka, B.L., Stevens, A.M., Parsek, M.R., Crone, T.J., and Greenberg, E.P. (1997). Mutational analysis of the *Vibrio fischeri* LuxI polypeptide: critical regions of an autoinducer synthase. J. Bacteriol. *179*, 4882–4887.

Hanzelka, B.L., Parsek, M.R., Val, D.L., Dunlap, P.V., Cronan, J.E.J., and Greenberg, E.P. (1999). Acylhomoserine lactone synthase activity of the *Vibrio fischeri* AinS protein. J. Bacteriol. *181*, 5766–5770.

Hentzer, M., Riedel, K., Rasmussen, T.B., Heydorn, A., Andersen, J.B., Parsek, M.R., Rice, S.A., Eberl, L., Molin, S., Hoiby, N., et al. (2002). Inhibition of quorum sensing in *Pseudomonas aeruginosa* biofilm bacteria by a halogenated furanone compound. Microbiology *148*, 87–102.

Hickman, A.B., Klein, D.C., and Dyda, F. (1999a). Melatonin biosynthesis: the structure of serotonin N-acetyltransferase at 2.5 Å resolution suggests a catalytic mechanism. Mol. Cell *3*, 23–32.

Hickman, A.B., Namboodiri, M.A., Klein, D.C., and Dyda, F. (1999b). The structural basis of ordered substrate binding by serotonin N-acetyltransferase: enzyme complex at 1.8 Å resolution with a bisubstrate analog. Cell *97*, 361–369.

Holm, L., and Sander, C. (1996). Mapping the protein universe. Science *273*, 595–602.

Izard, T., and Geerlof, A. (1999). The crystal structure of a novel bacterial adenylyltransferase reveals half of sites reactivity. EMBO J. *18*, 2021–2030.

Jones, T.A., Zou, J.Y., Cowan, S.W., and Kjelgaard, M. (1991). Improved methods for building protein models in electron density maps and the location of errors in these models. Acta Crystallogr. *A47*, 110–119.

Kanamaru, K., Tatsuno, I., Tobe, T., and Sasakawa, C. (2000). SdiA, an *Escherichia coli* homologue of quorum-sensing regulators, controls the expression of virulence factors in enterohaemorrhagic *Escherichia coli* O157: H7. Mol. Microbiol. *38*, 805–816.

Kraulis, P.J. (1991). MOLSCRIPT: a program to produce both detailed and schematic plots of protein structures. J. Appl. Crystallogr. *24*, 946–950.

Kuo, A., Blough, N.V., and Dunlap, P.V. (1994). Multiple N-acyl-L-homoserine lactone autoinducers of luminescence in the marine symbiotic bacterium *Vibrio-fischeri*. J. Bacteriol. *176*, 7558–7565.

Laskowski, R.A. (1993). PROCHECK: a program to check the stereochemical quality of protein structures. J. Appl. Crystallogr. *26*, 283–291.

Leadbetter, J.R., and Greenberg, E.P. (2000). Metabolism of acylhomoserine lactone quorum-sensing signals by Variovorax paradoxus. J. Bacteriol. *182*, 6921–6926.

Lewenza, S., and Sokol, P.A. (2001). Regulation of ornibactin biosynthesis and N-acyl-L-homoserine lactone production by CepR in *Burkholderia cepacia*. J. Bacteriol. *183*, 2212–2218.

Lewis, H.A., Furlong, E.B., Laubert, B., Eroshkina, G.A., Batiyenko, Y., Adams, J.M., Bergseid, M.G., Marsh, C.D., Peat, T.S., Sanderson, W.E., et al. (2001). A structural genomics approach to the study of quorum sensing: crystal structures of three LuxS orthologs. Structure *9*, 527–537.

Lithgow, J.K., Wilkinson, A., Hardman, A., Rodelas, B., Wisniewski-Dye, F., Williams, P., and Downie, J.A. (2000). The regulatory locus cinRI in *Rhizobium leguminosarum* controls a network of quorum-sensing loci. Mol. Microbiol. *37*, 81–97.

Mäe, A., Montesano, M., Koiv, V., and Palva, E.T. (2001). Transgenic plants producing the bacterial pheromone N-acyl-homoserine lactone exhibit enhanced resistance to the bacterial phytopathogen *Erwinia carotovora*. Mol. Plant Microbe Interact. *14*, 1035–1042.

McClean, K.H., Winson, M.K., Fish, L., Taylor, A., Chhabra, S.R., Camara, M., Daykin, M., Lamb, J.H., Swift, S., Bycroft, B.W., et al. (1997). Quorum sensing and *Chromobacterium violaceum*: exploitation of violacein production and inhibition for the detection of N-acylhomoserine lactones. Microbiology *143*, 3703–3711.

Moré, M.I., Finger, L.D., Stryker, J.L., Fuqua, C., Eberhard, A., and Winans, S.C. (1996). Enzymatic synthesis of a quorum-sensing autoinducer through use of defined substrates. Science *272*, 1655–1658.

Nicholls, A., Bharadwaj, R., and Honig, B. (1993). GRASP-graphical representation and analysis of surface properties. Biophys. J. *64*, A166.

Obsil, T., Ghirlando, R., Klein, D.C., Ganguly, S., and Dyda, F. (2001). Crystal structure of the 14-3-3zeta:serotonin *N*-acetyltransferase complex. A role for scaffolding in enzyme regulation. Cell *105*, 257–267.

Parsek, M.R., and Greenberg, E.P. (2000). Acyl-homoserine lactone

quorum sensing in Gram-negative bacteria: a signaling mechanism involved in the association with higher organisms. Proc. Natl. Acad. Sci. USA *97*, 8789–8793.

Parsek, M.R., Schaefer, A.L., and Greenberg, E.P. (1997). Analysis of random and site-directed mutations in *rhl*I, a *Pseudomonas aeruginosa* gene encoding an acyl homoserine lactone synthase. Mol. Microbiol. *26*, 301–310.

Parsek, M.R., Val, D.L., Hanzelka, B.L., Cronan, J.E.J., and Greenberg, E.P. (1999). Acyl homoserine-lactone quorum-sensing signal generation. Proc. Natl. Acad. Sci. USA *96*, 4360–4365.

Pearson, J.P., Van Delden, C., and Iglewski, B.H. (1999). Active efflux and diffusion are involved in transport of *Pseudomonas aeruginosa* cell-to-cell signals. J. Bacteriol. *181*, 1203–1210.

Puskas, A., Greenberg, E.P., Kaplan, S., and Schaefer, A.L. (1997). A quorum-sensing system in the free-living photosynthetic bacterium *Rhodobacter sphaeroides*. J. Bacteriol. *179*, 7530–7537.

Rojas, J.R., Trievel, R.C., Zhou, J., Mo, Y., Berger, S.L., Allis, C.D., and Marmorstein, R. (1999). Structure of *Tetrahymena* GCN5 bound to coenzyme A and a histone H3 peptide. Nature *401*, 93–98.

Rumbaugh, K.P., Griswold, J.A., Iglewski, B.H., and Hamood, A.N. (1999). Contribution of quorum sensing to the virulence of *Pseudomonas aeruginosa* in burn wound infections. Infect. Immun. *67*, 5853–5862.

Sitnikov, D.M., Schineller, J.B., and Baldwin, T.O. (1995). Transcriptional regulation of bioluminesence genes from *Vibrio fischeri*. Mol. Microbiol. *17*, 801–812.

Studier, F.W., Rosenberg, A.H., Dunn, J.J., and Dubendorff, J.W. (1990). Use of the T7 RNA polymerase to direct expression of cloned genes. Methods Enzymol. *185*, 60–89.

Swift, S., Karlyshev, A.V., Fish, L., Durant, E.I., Winson, M.K., Chhabra, S., Williams, P., Macintyre, S., and Stewart, G.S.A.B. (1997). Quorum sensing in *Aeromonas salmonicida*: identification of the LuxRI homologs AhyRI and AsaRI and their cognate *N*-acylhomoserine lactone signal molecules. J. Bacteriol. *179*, 5271–5281.

Swift, S., Williams, P., and Stewart, G.S.A.B. (1999). *N*-acylhomoserine lactones and quorum sensing in proteobacteria. In Cell-Cell Communication in Bacteria., G. Dunny, and S.C. Winans, eds. (AMS Press.), pp. 291–313.

Tang, H.B., DiMango, E., Bryan, R., Gambello, M., Iglewski, B.H., Goldberg, J.B., and Prince, A. (1996). Contribution of specific *Pseudomonas aeruginosa* virulence factors to pathogenesis of pneumonia in a neonatal mouse model of infection. Infect. Immun. *64*, 37–43.

Tanner, K.G., Trievel, R.C., Huo, M.-H., Howard, R.M., Berger, S.L., Allis, C.D., Marmorstein, R., and Denu, J.M. (1999). Catalytic mechanism and function of invariant glutamic acid 173 from the histone acetyltransferase GCN5 transcriptional coactivator. J. Biol. Chem. *274*, 18157–18160.

Teplitski, M., Robinson, J.B., and Bauer, W.D. (2000). Plants secrete substances that mimic bacterial N-acyl homoserine lactone signal activities and affect population density-dependent behaviors in associated bacteria. Mol. Plant Microbe Interact. *13*, 637–648.

Val, D.L., and Cronan, J.E.J. (1998). In vivo evidence that S-adenosylmethionine and fatty acid synthesis intermediates are the substrates for the LuxI family of autoinducer synthases. J. Bacteriol. *180*, 2644–2651.

Watson, W.T., Murphy, F.V., Gould, T.A., Jambeck, P., Val, D.L., Cronan, J.E., Beck von Bodman, S., and Churchill, M.E.A. (2001). Crystallization and rhenium MAD phasing of the acyl-homoserine lactone synthase EsaI. Acta Crystallogr. D*57*, 1945–1949.

Welch, M., Todd, D.E., Whitehead, N.A., McGowan, S.J., Bycroft, B.W., and Salmond, G.P.C. (2000). N-acyl homoserine lactone binding to the CarR receptor determines quorum-sensing specificity in Erwinia. EMBO J. *19*, 631–641.

Whitehead, N.A., Barnard, A.M., Slater, H., Simpson, N.J., and Salmond, G.P. (2001). Quorum sensing in Gram-negative bacteria. FEMS Microbiol. Rev. *25*, 365–404.

Zhu, J., and Winans, S.C. (2001). The quorum-sensing transcriptional regulator TraR requires its cognate signaling ligand for protein folding, protease resistance, and dimerization. Proc. Natl. Acad. Sci. USA *98*, 1507–1512.